2003

Dip effect in ac susceptibility due to surface barrier with flux creep

X. Leng
Nanjing University, China

Shichao Ding
University of Wollongong, sding@uow.edu.au

Y. Liu
Nanjing University, China

Z. H. Wang
Nanjing University, China

Hua-Kun Liu
University of Wollongong, hua@uow.edu.au

See next page for additional authors

Publication Details

This article was originally published as: Leng, X, Ding, SY, Liu, Y, Wang, ZH, Liu, HK & Dou, SX, Dip effect in ac susceptibility due to surface barrier with flux creep, Physical Review B, 2003, 68, 214511. Copyright 2003 American Physical Society. The original journal can be found here.

Authors
X. Leng, Shichao Ding, Y. Liu, Z. H. Wang, Hua-Kun Liu, and S. X. Dou

PHYSICAL REVIEW B **68**, 214511 (2003)

Dip effect in ac susceptibility due to surface barrier with flux creep

X. Leng, S. Y. Ding,* Y. Liu, and Z. H. Wang
National Laboratory of Solid State Microstructures, Department of Physics, Nanjing University, Nanjing 210093, Peoples Republic of China

H. K. Liu and S. X. Dou
Institute for Superconducting and Electronic Materials, University of Wollongong, Wollongong NSW 2522, Australia
(Received 5 June 2003; revised manuscript received 11 September 2003; published 18 December 2003)

A model is proposed to describe the effect of surface barrier (SB) on ac susceptibility (ACS) and a different kind of dip effect (DE) in ACS is observed. Simulation based on this model with flux creep reveals two dips in ACS curve, one at temperature $T'_{\rm d}$ in real part χ' and the other at temperature $T''_{\rm d}$ in imaginary part χ''. These two dips are different from the ones resulting from the peak effect in critical current density $j_{\rm c}$, where the dips in χ' and χ'' occur at the same temperature $T_{\rm p}$. The DE is also characterized by a large χ'' and a large $|\chi'(T'_{\rm d})|$. The ACS curves for single crystals $Bi_2Sr_2CaCu_2O_8$ have been observed and compared with the DE in $YBa_2Cu_3O_7$ samples, confirming the numerical results. It is also shown that when flux creep is absent only kinks appear in χ' and χ'' for a sample with SB.

DOI: 10.1103/PhysRevB.68.214511 PACS number(s): 74.25.Sv, 74.25.Qt, 74.72.Hs, 74.25.Op

I. INTRODUCTION

There have been numbers of papers concerning the surface barriers (SB's) of the conventional and high-temperature superconductors (HTSC's).[1–18] The Bean-Livingston barrier,[1–9] the geometrical barrier,[9–13] and the surface pinning barrier[14,15] all belong to SB's. The Bean-Livingston barrier results from the competition between vortex attraction to the surface (''mirror image'' effect) and its repulsion from the surface due to the vortex interaction with the reversible shielding current. The geometrical barrier also results from the competition of two interactions. One is the Lorentz force caused by the Meissner screening current, which drives the vortex line towards the center of a sample (usually a thin film, in perpendicular field). The second one is that for a vortex at the very edge or corners of the sample, its line tension will keep it near the edge, which opposes the inward Lorentz force. As the applied field increases, the two penetrating vortex segments will finally join together then the line tension no longer produces a significant outer force. As for the surface pinning, the surface defects will cause stronger surface pinning force, which means that the surface critical current density $j_{\rm cs}$ will be larger than the inside one ($j_{\rm cb}$). In some HTSC's such as Ag-Bi2212 tapes the higher $j_{\rm cs}$ may result from the fewer weak links and the better quality in the surface zone.

Several experimental methods have been developed for SB studies. For example, in hysteresis-loop measurements, smaller magnetization in the descending branch has been found and considered as a ''fingerprint'' of SB's.[4,6,11] For another example, a crossover on the magnetic relaxation rate curve $dM/d\ln(t)$ was predicted and observed as an effect of SB's.[14,18] Recently, the current density profiles of Bi-based HTSC crystals and silver-sheathed tapes have been measured with Hall sensors[7,12,22–25] and the distributions of magnetic field have been visualized clearly by means of magneto-optical images.[3,19–21] These experiments show that there exist surface zones with much higher $j_{\rm c}$ than the inside.

ac susceptibility (ACS) $\chi_n=\chi'_n+i\chi''_n$ is also a powerful tool when we study flux dynamics.[13,16,17,26–31] For example, it has been used to study the so-called $j_{\rm c}$ peak effect (PE), where the dips in $\chi(T)$ is considered as the peaks in $j_{\rm c}$ according to the following equation[27,28]:

$$j_{\rm c}=\frac{B_{\rm ac}}{2\mu_0 d(1-|\chi'|)}=\frac{2B_{\rm ac}}{3\mu_0 d(|\chi''|)}, \quad \left(\frac{B_{\rm ac}}{\mu_0 d}\leqslant j_{\rm c}\right),$$

where $B_{\rm ac}$ and d are amplitude of ac field and half-width of the sample, respectively. For another example, a well-oxygenated surface with higher $j_{\rm c}$ has been observed in Yttrium barium copper oxide (YBCO) single crystal using Campbell's method.[29–31]

For HTSC's, flux creep is significant due to the high operating temperature and small activation energy U that usually depends on current density. So the critical state models, e.g., the Bean model,[2,8] are no longer proper. Instead, nonlinear flux creep models are effective in the study of flux dynamics. Therefore, we will adopt a nonlinear flux creep model in the simulation below and the critical state case will be calculated for comparison.

In this paper, we propose a phenomenological model to describe SB and study the effect of SB on ACS. The logarithmic flux creep model is used in our simulation. In order to examine the simulation results, ACS curves are measured and compared with the numerical results.

II. MODEL AND SIMULATION

Let a sample be an infinite slab consisted of two $j_{\rm c}$ such that the higher one ($j_{\rm cs}$) describes SB while the lower one ($j_{\rm cb}$) is a reflection of bulk pinning (Fig. 1). The bulk width is $d_{\rm b}$ whose dimension is in millimeter for a typical bulk sample and in micrometer for a thin film. The surface width $d_{\rm s}$ can be compared with the penetration depth λ for the Bean-Livingston barrier and geometrical barriers whereas is a relatively broad zone for the surface pinning barrier. There-

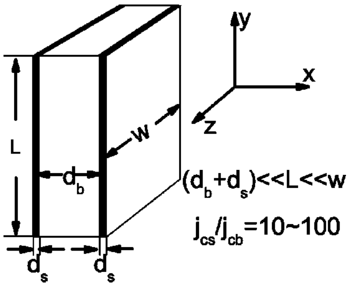

FIG. 1. Schematic sketch for our model. The surfaces are blacked and have critical current density j_{cs}, while the bulk zone has weak pinning with j_{cb}. The strength of surface barrier is adjusted by j_{cs}/j_{cb}, and the width of surface is adjusted by d_s/d_b.

fore, we can simulate the SB by properly choosing $d_b(1\ \mu\text{m}\sim1\ \text{mm})$ and d_s/d_b $(10^{-4}\sim10^{-1})$. In fact, though adjust d_s/d_b from 0.1 to 0.001 for $j_{cs}/j_{cb}=10\sim100$, the numerical results are almost the same. The nonlinear flux diffusion is described by the logarithmic barrier: $U(j)=U_0\ln|j_c/j|$, and thus the flux-line velocity is

$$v=v_0(j/j_c)\exp[-U(j)/(kT)]=v_0(j/j_c)|j/j_c|^n, \qquad (1)$$

where $n=U_0/(kT)$ and v_0 is the velocity at $U=0$. The factor j/j_c is introduced to provide a gradual crossover to flux flow regime, $v\propto j$, at $kT\gg U(j)$.[32] For simplification, we suppose $U_{0s}=U_{0b}=U_0$. From Eq. (1) the power law $E(j)=E_0(j/j_c)^{n+1}$ is obtained, which results in the Bean model for $(n+1)\to\infty$ and the Ohm law for $(n+1)=1$. Let the surfaces of the slab be in y-z plane, thickness d along the x axis, the applied field $B_a\|z$. Using the Maxwell equations, one gets the diffusion equation of flux line[33,34]

$$\frac{\partial B}{\partial t}=\frac{v_0}{(\mu_0 j_c)^{n+1}}\frac{\partial}{\partial x}\left[\left|\frac{\partial B}{\partial x}\right|^n\left(\frac{\partial B}{\partial x}\right)\left|B\right|\right]. \qquad (2)$$

The boundary and initial conditions are, respectively,

$$B(x=0,d;t)=B_{dc}+B_{ac}\sin(2\pi ft),$$

$$B(x,t=0)=B_{dc}.$$

The complex elementary ACS then can be calculated by

$$\chi=\chi'+i\chi''=\frac{1}{\pi B_{ac}}\int_0^{2\pi}\mu_0 M(t)\exp(i2\pi ft)d(2\pi ft), \qquad (3)$$

where the magnetization is

$$\mu_0 M(t)=\left[\frac{1}{d}\int_0^d B(x,t)\mathrm{d}x\right]-[B_{dc}+B_{ac}\sin(2\pi ft)]. \qquad (4)$$

The temperature and field dependence of the critical current density and apparent activation energy are supposed as follows, respectively,[35]

$$j_c(T,B)=j_{c0}\left[1+\left(\frac{T}{T_c}\right)^2\right]^{-1/2}\left[1-\left(\frac{T}{T_c}\right)^2\right]^{5/2}\frac{B_0}{B_0+|B|}, \qquad (5)$$

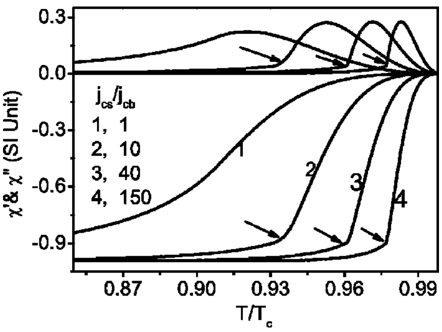

FIG. 2. Numerical ACS curves at different strengths of surface barrier (different j_{cs}/j_{cb}) for the critical state model. The kinks indicated by arrows reflect the influence of surface barrier on ACS without flux creep. $f=100$ Hz, $B_{dc}=1000$ Gs, $B_{ac}=10$ Gs, $d_s/d_b=0.1$.

$$U_0(T,B)=U_{00}\left[1-\left(\frac{T}{T_c}\right)^4\right]\frac{B_0}{B_0+|B|}. \qquad (6)$$

In the following we let $n_0=n(T=0,B=0)=5$, $v_0=1$ m/s,[32] $j_{cb}=5\times10^8$ A/m^2,[19] and $B_0=500$ Gs.

With the finite difference method, the nonlinear diffusion equation can be numerically solved and the implicit difference scheme is used for stability.

III. RESULTS AND DISCUSSIONS

A. Effect of SB without flux creep

We first study the influence of SB on ACS without flux creep which is the case of Eq. (1) at $n=\infty$, i.e., j is either 0 or j_c. Combining Eqs. (1)–(6), we calculate the ACS curves at different strengthes of SB and show a typical result in Fig. 2. One can see that with increasing SB, there appear kinks in $\chi'(T)$ and $\chi''(T)$ curves, as indicated by the arrows. This is a characteristic of surface pinning when the critical state mode is suitable. In addition, as the strength of SB increases, the $\chi'(T)$ and $\chi''(T)$ curves shift to higher temperatures and the transitions become sharper.

B. Effect of SB with flux creep

We now depict the influence of SB on ACS when flux creep is important. The complex $\chi(T)$ curves at different strength of SB and different DC fields are shown in Fig. 3 and Fig. 4, respectively. Several important features can be seen. First, instead of the kinks in the ACS curves for the critical state model, dips are found in both the real and imaginary parts of the ACS curves. The dip temperature T_d', at which $\chi'(T)$ dips, is different from the dip temperature T_d'', at which $\chi''(T)$ dips, as indicated by the arrows in Fig. 3. This is in contrast with the dips found in $\chi(T)$ curves resulting from the PE in j_c, where the dips in $\chi'(T)$ and $\chi''(T)$ take place at the same temperature T_p (see Refs. 28,36–38). The second feature is that the dip depth increases with SB until $|\chi'|>1$ around the dip temperature T_d', as seen in Fig. 3. To our knowledge, both the features have not been reported so far. The third feature is that the magnitude

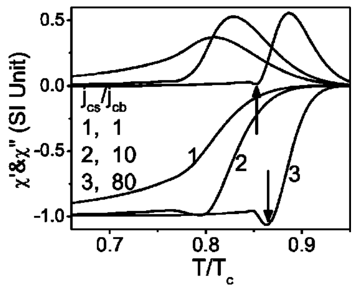

FIG. 3. Numerical ACS curves as a function of temperature for different strength of surface barrier with flux creep. Note that the dips in the real and imaginary parts of ACS take place at different temperatures, as indicated by arrows, showing the effect of surface pinning on ACS. $f=100$ Hz, $B_{\mathrm{dc}}=500$ Gs, $B_{\mathrm{ac}}=10$ Gs, $d_s/d_b=0.1$.

of χ'' with SB is apparently larger than the one caused only by bulk pinning, see Fig. 3 (also can be seen in Fig. 8). The last feature, as shown in Fig. 4 (also in Fig. 9), is that as dc field increases, the dip in $\chi'(T)$ broadens while its depth remains unchanged.

Since the $U(j,T)$ dependence used in our simulation is rather complicated, there is an important question that whether the dips result from the T dependence of $U(j)$ or will the dips remain for other T dependences of $U(j)$? To address this question, we keep T constant and simulate ACS as a function of B_{ac} as shown in Fig. 5. The dip effect (DE), as well as all the other features shown in Fig. 3 can be found here. These results indicate that the DE is an universal feature for the surface barrier with flux creep.

The DE in the $\chi-T(H)$ or $R-T(H)$ has been considered as a result of PE in j_c caused only by bulk pinning.[28,36–38] Therefore, our result reveals a different kind of DE originated from the SB with flux creep. However, it is easy to distinguish the two kinds of DE according to their different features as pointed out above.

To see why $|\chi'(T)|>1$ in the dip segment of ACS curves, we calculate the field distributions in a sample. The field evolution at $T=T_d'$ in the first and second periods of the AC field for $j_{\mathrm{cs}}/j_{\mathrm{cb}}=100$ are shown in Fig. 5. In the second period, a blacked area appears with the increasing applied field (see panel 6 of Fig. 6), which means though the applied field has reached the positive maximum, there are still many "negative flux lines" in the bulk zone of the sample. When the SB is strong enough the blacked area will be larger than the hatched one (causing $|\chi'|>1$) as shown in panels 4, 6, and 8 (Fig. 6). It is apparent that SB is a direct reason for these large numbers of "negative flux lines." That is to say, there is an "extra hysteresis" originated from the SB with flux creep. Naturally, with increasing SB at fixed bulk pinning (or equivalently, decreasing bulk pinning at fixed SB) the "negative flux lines" will increase as well, causing larger $|\chi'|$.

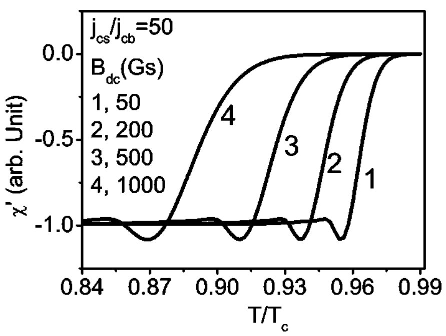

FIG. 4. Under the surface barrier model with flux creep, the real parts of the numerical ACS curves as a function of temperature at different dc fields. Note that when the dc field is increased, the dip in χ' broadens while its depth remains unchanged. $f=500$ Hz, $B_{\mathrm{ac}}=0.5$ Gs, $d_s/d_b=0.1$.

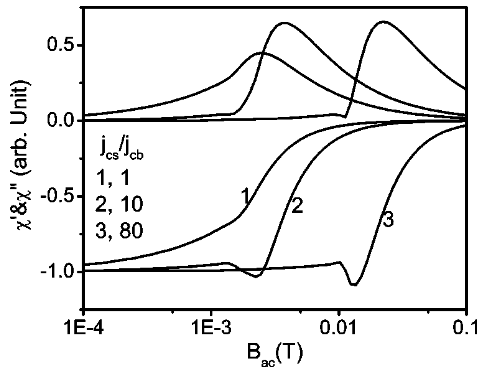

FIG. 5. Numerical $\chi(B_{\mathrm{ac}})$ curves at a constant temperature for different strength of surface barrier with flux creep. $f=100$ Hz, $B_{\mathrm{dc}}=0$, $T/T_c=0.9$, $d_s/d_b=0.1$.

The field distributions at different temperatures when the applied AC field reaches the positive maximum (i.e., panel 6 of Fig. 6) are shown in Fig. 7. In Fig. 7(a), where SB is absent, the field profile is similar to the usual distributions as seen in Ref. 35, where there is also the blacked area (negative flux lines) but is smaller than the hatched one, implying $|\chi'|\leqslant 1$. In contrast, in Fig. 7(b), the blacked area is larger than the hatched one as a result of SB, causing $|\chi'|>1$, as indicated by the lowest arrow.

It is noted that the ACS with SB is larger than the ACS without SB. We know that the imaginary part of ACS is

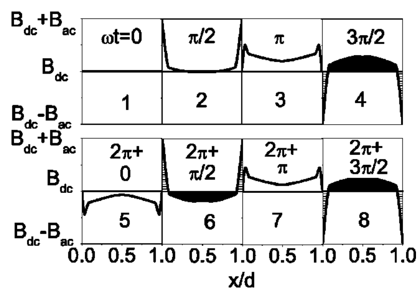

FIG. 6. The numerical field evolution inside a sample with surface barrier and flux creep at the dip temperature T_d' during the first ($2\pi f t=\omega t=0\sim 3\pi/2$) and second ($\omega t=2\pi+0\sim 2\pi+3\pi/2$) cycles of the applied ac field. The flux distributions of the successive cycles are basically the same as the second one. The reason why $|\chi'|>1$ is that the blacked area is greater than the hatched one (4, 6, 8). $f=100$ Hz, $B_{\mathrm{dc}}=500$ Gs, $B_{\mathrm{ac}}=10$ Gs, $j_{\mathrm{cs}}/j_{\mathrm{cb}}=100$, $d_s/d_b=0.1$.

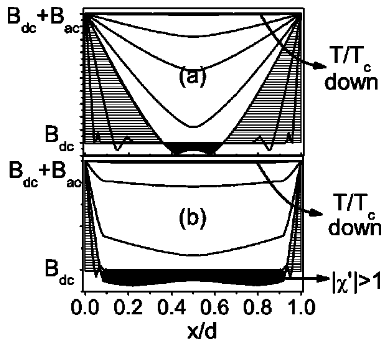

FIG. 7. The numerical field evolution inside a sample with flux creep at different temperatures when the applied field reached the positive maximum($\omega t=2n\pi+\pi/2$). (a) Without SB, the blacked area is smaller than the hatched one, causing $|\chi'|<1$. $f=100$ Hz, $B_{dc}=500$ Gs, $B_{ac}=10$ Gs; (b) With a SB ($j_{cs}/j_{cb}=100$), the blacked area is larger than the hatched one at temperature T_d', causing $|\chi'|>1$, as indicated by the lowest arrow. $f=100$ Hz, $B_{dc}=500$ Gs, $B_{ac}=10$ Gs, $d_s/d_b=0.1$.

proportional to the ac loss, i.e., the area of $M(B)$ hysteresis loop, and the real part is proportional to the magnitude of $M(B)$. Figure 7 shows that M with SB [Fig. 7(b)] is larger than M without SB [Fig. 7(a)]. So it is reasonable that both χ' and χ'' with SB are larger than the ones without SB.

It has been pointed out that the two dips occur at different temperatures T_d' and T_d'' (or different fields in Fig. 5). It is well known that χ'' and the ratio $|\chi''/\chi'|$ depend on the material equation [Eq. (1)] of the sample. For examples, for a normal metal or a superconductor in flux flow regime, $n=0$ in Eq. (1), $\chi''_{\max}\geqslant 0.41$; for the Bean model, $n=\infty$, $\chi''_{max}\approx 0.21$ for a slab, independent of j_c. Now, for a superconductor with SB and flux creep, the material equation is no longer Eq. (1) but a combination of two kinds of Eq. (1) with j_{cs} and j_{cb}. Therefore, χ'', $|\chi''/\chi'|$, and the dips will have their own features as depicted above.

IV. EXPERIMENT

A high quality single crystal $Bi_2Sr_2CaCu_2O_8$ (Bi2212) of $0.75\times 0.5\times 0.015$ cm^3 was prepared for our experiments and the results are shown in Figs. 8 and 9.

The experimental ACS curves results are very similar to the numerical ones of a sample with SB and flux creep (see Figs. 3 and 4). For example, the dips in $\chi'(T)$ and $\chi''(T)$ are at different temperatures T_d' and T_d'', respectively, as indicated by the arrows. Second, a large peak with a height of 0.5 can be seen in the $\chi''(T)$ curve. The third one is that with increasing dc field, the dip width of $\chi'(T)$ increases while their depth remains unchanged. All these are strong evidence that there exist SB's in $Bi_2Sr_2CaCu_2O_8$, which agrees well with the experimental findings as pointed above.[3,7,12,19–25] Thus the experimental results of Bi2212 not only support our SB model but also show there is a different kind of DE originated from SB with flux creep.

In contrast, it has been reported that for YBCO, the dips in the real and imaginary parts of ACS take place at the same temperature T_p, for example, see Fig. 1 of Ref. 36; and also

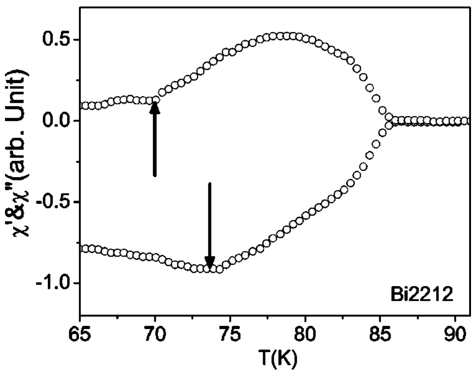

FIG. 8. The experimental ACS curves for Bi2212. It is clear that two dips marked by arrows occur at different temperatures and a large broad peak appears in $\chi''(T)$ curve, conforming the numerical results (see Fig. 3). $f=500$ Hz, $B_{dc}=170$ Gs and $B_{ac}=5$ Gs.

in Fig. 2 of Ref. 36, it can be seen that though the dc field increases from 1 to 7 T, the experimental dip width of YBCO is almost unchanged while the dip depth decreases, in contrast with the DE of SB. There have been also numbers of papers that have reported two dips at the same temperature T_p in χ' and χ'' for YBCO, which are considered as the results of the PE in j_c caused only by bulk pinning.[28,37,38] So the experimental results of YBCO strongly demonstrates that the SB is not important in YBCO and there do exist two kinds of DE in HTSC's.

The feature $|\chi'(T)|>1$ in the dip segment has not been found in our experimental results, which may result from some reasons as follows. According to the numerical results, this feature can only be seen in a sample with much high surface strength. See Fig. 3, when j_{cs} is ten times larger than j_{cb}, $|\chi'|$ is always less than 1 though the DE can be clearly seen. So perhaps the surface strength of our sample is not large enough to show the feature of $|\chi'(T)|>1$. And also the demagnetization factor is not corrected for our experimental data. So the experimental data may be more suitable for qualitative analysis than for quantitative analysis.

From Figs. 8 and 9 we learn that the SB can be experi-

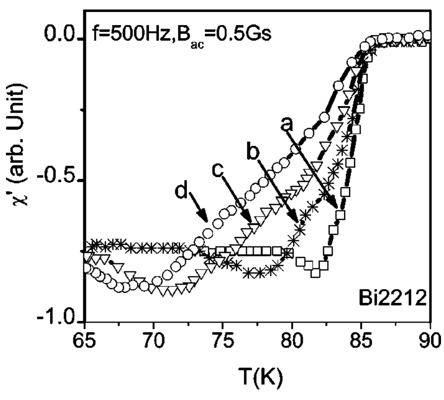

FIG. 9. The real part of experimental ACS curves for Bi2212 at different dc fields. The dip width increases with dc field while its depth is almost unchanged, consistent with the numerical results (see Fig. 4). B_{dc}: a=50 Gs, b=90 Gs, c=200 Gs, d=300 Gs.

mentally probed and distinguished by ACS measurement besides the others such as magneto-optical images and Hall arrays. Combining the numerical and experimental results, we conclude that flux creep and SB are two necessary conditions for the DE. In some pure layered Bi2212 single crystals, the relatively weak bulk pinning and high operating temperature meet the two conditions. On the contrary, YBCO is more isotropic and has stronger bulk pinning, and thus the importance of SB decreases. Therefore, It is possible that the large j_{cb} and thus the small $j_{\mathrm{cs}}/j_{\mathrm{cb}}$ cause the SB in YBCO too weak to be probed by common ACS measurement.

V. SUMMARY

We have proposed a model to describe the effect of surface barrier on ACS. The ACS curves have been calculated with and without flux creep, respectively. When flux creep is important, a different kind of DE is numerically observed in ACS curves. Several features of the DE have been found and compared with the ones resulting from the PE in j_{c} caused only by bulk pinning. The most important one is that the dips in the real and imaginary parts of ACS curves occur at different temperatures T'_{d} and T''_{d}, respectively, in contrast with the dips resulting from the PE in j_{c}. The DE is also characterized by a larger χ''. In addition, the dip temperature T'_{d}, T''_{d} and the dip depth all increase with SB and $|\chi'(T'_{\mathrm{d}})|$ will be larger than 1 if the SB is strong enough. When flux creep is so weak that the critical state model is suitable, kinks instead of dips take place in $\chi'(T)$ and $\chi''(T)$ for a sample with SB. The numerical results are supported not only by our own experimental curves but also by references.

ACKNOWLEDGMENTS

The Ministry of Science and Technology of China (Grant No. NKBRSFG1999-0646) and NNSFC (Grant No. 19994016) support the work.

*Email address: Syding@netra.nju.edu.cn

[1] C.P. Bean and J.D. Livingston, Phys. Rev. Lett. **12**, 14 (1964).
[2] J.R. Clem, J. Appl. Phys. **50**, 3518 (1979).
[3] L. Burlachkov, V.B. Geshkenbein, A.E. Koshelev, A.I. Larkin, and V.M. Vinokur, Phys. Rev. B **50**, 16 770 (1994).
[4] L. Burlachkov, Phys. Rev. B **47**, 8056 (1993).
[5] L. Burlachkov, A.E. Koshelev, and V.M. Vinokur, Phys. Rev. B **54**, 6750 (1996).
[6] L. Burlachkov, M. Konczykowski, Y. Yeshurun, and F. Holtzberg, J. Appl. Phys. **70**, 5759 (1991).
[7] M.S. James, S.T. Stoddart, S.J. Bending, S. Aukkaravittayapun, P.J. King, and M. Henini, Phys. Rev. B **56**, 5771 (1997).
[8] S. Tochihara, H. Yasuoka, and H. Mazaki, Physica C **295**, 101 (1998).
[9] M. Benkraouda and J.R. Clem, Phys. Rev. B **58**, 15 103 (1998).
[10] E.H. Brandt, Phys. Rev. Lett. **71**, 2821 (1993); Phys. Rev. B **60**, 11 939 (1999).
[11] M. Benkraouda and J.R. Clem, Phys. Rev. B **53**, 5716 (1996).
[12] E. Zeldov, A.I. Larkin, V.B. Geshkenbein, M. Konczykowski, D. Majer, B. Khaykovich, V.M. Vinokur, and H. Shtrikman, Phys. Rev. Lett. **73**, 1428 (1994).
[13] G.M. Maksimova, D.Yu. Vodolazov, and I.L. Maksimov, Physica C **356**, 67 (2001).
[14] S.T. Weir, W.J. Nellis, Y. Dalichaouch, B.W. Lee M.B. Maple, J.Z. Liu, and R.N. Shelton, Phys. Rev. B **43**, 3034 (1991).
[15] E. Sheriff, R. Prozorov, Y. Yeshurun, A. Shaulov, G. Koren, and C. Chabaud-Villard, J. Appl. Phys. **82**, 4417 (1997).
[16] C.J. van der Beek, M.V. Indenbom, G.D'. Anna, and W. Benoit, Physica C **258**, 105 (1996).
[17] C.J. van der Beek, S. Colson, M.V. Indenbom, and M. Konczykowski, Phys. Rev. Lett. **84**, 4196 (2000).
[18] Y. Yeshurun, A.P. Malozemoff, A. Shaulov, Rev. Mod. Phys. **68**, 911 (1996).
[19] K. Kawano, A. Oota, K. Fukuta, T. Higuchi, and H. Fujimoto, Cryogenics **39**, 853 (1999).
[20] A.V. Bobyl, D.V. Shantsev, Y.M. Galperin, T.H. Johansen, M. Baziljevich, and S.F. Karmanenko, Supercond. Sci. Technol. **15**, 82 (2002).
[21] Y. Radzyner, Y. Abulafia, Y. Yeshurun, T. Staiger, and G. Fuchs, Physica C **307**, 165176 (1998).
[22] D.T. Fuchs, E. Zeldov, M. Rappaport, T. Tamegai, S. Ooi, and H. Shtrikman, Nature (London) **391**, 373 (1998); D.T. Fuchs *et al.*, Phys. Rev. Lett. **80**, 4971 (1998).
[23] Y. Paltiel, *et al.*, Nature (London) **403**, 398 (2000).
[24] J. Herrmann, N. Savvides, K.H. Muller, R. Zhao, G. McCaughey, F. Darmann, and M. Apperley, Physica C **305**, 114 (1998).
[25] Y. Paltiel, D.T. Fuchs, E. Zeldov, Y.N. Myasoedov, H. Shtrikman, M.L. Rappaport, and E.Y. Andrei, Phys. Rev. B **58**, 14 763 (1998).
[26] Y. Ge, S.Y. Ding, Q. Ding, C. Ren, L. Qiu, F.Y. Ling, X.X. Yao, Y.X. Fu, and C.B. Cai, Physica C **292**, 59 (1997).
[27] R.B. Goldfarb, M. Lelental, and C.A. Tompson, in *Magnetic Susceptibility of Superconductors and Other Spin Systems*, edited by R.A. Hein, T.L. Francavilla, and D.H. Liebenberg (Plenum, New York, 1991), pp. 49–80.
[28] X.S. Ling and J.I. Budnick, in *Magnetic Susceptibility of Superconductors and Other Spin Systems*, edited by R.A. Hein, T.L. Francavilla, and D.H. Liebenberg (Plenum, New York, 1991), pp. 377.
[29] A.M. Campbell, J. Phys. C **4**, 3186 (1971).
[30] F. Gömöry and S. Takács, Superlattices Microstruct., **21**, 219 (1997).
[31] F. Gömöry, Supercond. Sci. Technol. **10**, 523 (1997).
[32] V.M. Vinokur, M.V. Feigel'man, and V.B. Geshkenbein, Phys. Rev. Lett. **67**, 915 (1991).
[33] D.V. Shantsev, Y.M. Galperin, and T.H. Johansen, Phys. Rev. B **65**, 184512 (2002).
[34] Y. Liu, S.Y. Ding, X. Leng, H. Luo, L. Qiu, Z.H. Wang, and L.Z. Lin, Phys. Rev. B **66**, 144510 (2002).
[35] M.J. Qin and X.X. Yao, Phys. Rev. B **54**, 7536 (1996).
[36] J. Shi, X.S. Ling, R. Liang, D.A. Bomn, and W.N. Hardy, Phys. Rev. B **60**, R12593 (1999).
[37] P. Zhang, S.Y. Ding, X.F. Wu, L. Qiu, Z.H. Wang, C. Ren, S.A. Aruna, X.X. Yao, and J. Shi, Phys. Rev. B **62**, 5374 (2000).
[38] S.O. Valenzuela and V. Bekeris, Phys. Rev. Lett. **84**, 4200 (2000).